

Density induced BCS-Bose evolution in gated two-dimensional superconductors: The Berezinskii-Kosterlitz-Thouless transition as a function of carrier density

Tingting Shi^{1,2}, Wei Zhang^{1,*} and C. A. R. Sá de Melo^{2†}

¹ *Department of Physics, Renmin University of China, Beijing 100872, China and*

² *School of Physics, Georgia Institute of Technology, Atlanta, Georgia 30332, USA*

We discuss the evolution from BCS to Bose superconductivity versus carrier density in gated two-dimensional s -wave superconductors. We investigate the carrier density dependence of the critical temperature, superfluid density, order parameter, chemical potential and pair size. We show that the transition from the normal to the superconducting state is controlled by the Berezinskii-Kosterlitz-Thouless vortex-antivortex pairing mechanism, and that the evolution from high carrier density (BCS pairing) to low carrier density (Bose pairing) is just a crossover in s -wave systems. We compare our results to recent experiments on the superconductor Li_xZrNCl , a lithium-intercalated layered nitride, and obtain very good quantitative agreement at low and intermediate densities.

Introduction: The physics of two-dimensional (2D) superconductors is a fascinating subject with a long history [1]. The theoretical prediction that 2D Fermi systems can exhibit superconductivity can be inferred from the seminal papers of Berezinskii [2], Kosterlitz and Thouless [3], where the mechanism of vortex-antivortex unbinding was proposed. The topological nature of the superconducting transition in two dimensions at fixed carrier density was unveiled in experimental studies of thin films [4, 5], which provided strong evidence for the Berezinskii-Kosterlitz-Thouless (BKT) transition and vortex-antivortex unbinding [6].

Chemical substitutions or atom deficiencies in 2D materials can change carrier density, but very often they also introduce disorder and inhomogeneous doping, creating difficulties in the interpretation of experimental data and phase diagrams. A way to circumvent such difficulties is to study 2D systems via electrostatic doping, where the carrier density n can be tuned from a minimum n_{\min} to a maximum n_{\max} value. It was theoretically proposed that topological quantum phase transitions occur during the evolution from BCS to Bose pairing in 2D d - and p -wave superfluids and superconductors as a function of density or interaction strength [7–10]. However, experiments that used electrostatic doping in 2D d -wave superconductors (cuprates) [11, 12] did not investigate the existence of a quantum critical point from gapless to gapped from high (BCS pairing) to low (Bose pairing) density of carriers, but indicated that phase fluctuations play an important role in determining the critical temperature at low carrier densities. This experimental observation was in agreement with a theoretical argument that classical phase fluctuations were very important in establishing an upper bound for the critical temperature of 2D superconductors with small superfluid density [13]. Furthermore, these early experiments provided support to the viewpoint that the relation between the critical temperature T_c and the muon depolarization rate in cuprate superconductors [14, 15] should be reinterpreted as an upper bound on T_c given by the ordering temperature

for phase fluctuations [13].

For single band 2D superfluids and superconductors with parabolic bands, it was shown explicitly that this upper bound for the critical temperature $T_c = T_{\text{BKT}}$ is exactly one-eighth of the Fermi energy ε_F , that is, $T_{\text{BKT}} \leq \varepsilon_F/8 = 0.125\varepsilon_F$ [16] in units where $\hbar = k_B = 1$. Such a general relation is obtained rather trivially from the BKT transition temperature $T_{\text{BKT}} = \pi\rho_s(T_{\text{BKT}})/2$, where ρ_s is the superfluid density. It is sufficient to notice that, at any temperature T , $\rho_s(T)$ cannot exceed $n/(4m)$, where n is the carrier density and m is the carrier effective mass. Physically, this bound is the ratio between the maximum fermion pair density ($n/2$) and the fermion pair mass $2m$ and reflects the Ferrell-Glover-Tinkham [17–19] optical conductivity sum rule. The same bound is valid even when the superfluid density tensor is anisotropic or when spin-orbit effects are included [20, 21].

Experiments seeking to study the evolution from BCS to Bose pairing in essentially 2D superconductors like FeSe [22–24], twisted bilayer graphene [25, 26], and layered nitrides [27] have been attempted, but only very recently it has been shown that in Li_xZrNCl , a lithium-intercalated layered nitride, the electrolyte LiClO_4 can dope a 2D layer of ZrNCl with Lithium ions via a gate voltage V_G , over a range of nearly two orders of magnitude [28]. Because of this doping tunability, this technique potentially allows for the study of the evolution from BCS (high carrier density) to the Bose (low carrier density) superconductivity in 2D systems as discussed theoretically in the context of ultracold fermions [16]. In this paper, we show that a theory involving phase fluctuations for 2D s -wave superconductors leads to critical temperature and order parameter modulus in good agreement with experimental results for Li_xZrNCl [28] as the system evolves from BCS to Bose pairing in the relevant carrier concentration range. Furthermore, we extract from experimental data the effective mass of the charge carriers, as well as, the magnitude and range of the effective two-body interaction between them.

Hamiltonian: We use a two-band continuum model of fermion with identical parabolic bands centered at points K and K' of the Brillouin zone of Li_xZrNCl . Since the two bands are identical, the effective mass of the carriers in each band is m and density of carriers per band is $n = k_F^2/2\pi$. Furthermore, we take the interactions to be the same in both bands and assume that the two bands are independent. In this case, it is sufficient to consider the Hamiltonian per band. Thus, we start from the Hamiltonian density per band ($\hbar = k_B = 1$) $\mathcal{H}(\mathbf{r}) = \mathcal{H}_K(\mathbf{r}) + \mathcal{H}_I(\mathbf{r})$, where the kinetic energy density with respect to the chemical potential μ is

$$\mathcal{H}_K(\mathbf{r}) = \sum_s \psi_s^\dagger(\mathbf{r}) \left[-\frac{\nabla^2}{2m} - \mu \right] \psi_s(\mathbf{r}), \quad (1)$$

and the interaction energy density is

$$\mathcal{H}_I(\mathbf{r}) = \int d^2\mathbf{r}' V(\mathbf{r}, \mathbf{r}') \psi_\uparrow^\dagger(\mathbf{r}) \psi_\downarrow^\dagger(\mathbf{r}') \psi_\downarrow(\mathbf{r}') \psi_\uparrow(\mathbf{r}) \quad (2)$$

with $V(\mathbf{r}, \mathbf{r}') = -V_s g(|\mathbf{r} - \mathbf{r}'|/R)$. Here, V_s is the magnitude of the s -wave attractive interaction with dimension of energy, and $g(|\mathbf{r} - \mathbf{r}'|/R)$ is a dimensionless function with range R . The field operator $\psi_s^\dagger(\mathbf{r})$ creates a fermion with spin projection s at position \mathbf{r} . The Hamiltonian $H = \int d^2\mathbf{r} \mathcal{H}(\mathbf{r})$ has three microscopic parameters: the effective mass m , the interaction strength V_s and the interaction range R . In momentum space, the Hamiltonian reads

$$H = \sum_{\mathbf{k}, s} \xi_{\mathbf{k}} \psi_{\mathbf{k}, s}^\dagger \psi_{\mathbf{k}, s} + \sum_{\mathbf{k}, \mathbf{k}', \mathbf{q}} V_{\mathbf{k}\mathbf{k}'} b_{\mathbf{k}\mathbf{q}}^\dagger b_{\mathbf{k}'\mathbf{q}}, \quad (3)$$

where $b_{\mathbf{k}\mathbf{q}} = \psi_{-\mathbf{k}+\mathbf{q}/2, \downarrow} \psi_{\mathbf{k}+\mathbf{q}/2, \uparrow}$ is the pairing operator and $\xi_{\mathbf{k}} = \varepsilon_{\mathbf{k}} - \mu$, with energy dispersion $\varepsilon_{\mathbf{k}} = \mathbf{k}^2/2m$. Following standard procedure [7], we obtain a separable interparticle potential in momentum space

$$V_{\mathbf{k}\mathbf{k}'} = -V_s \Gamma_s(\mathbf{k}) \Gamma_s(\mathbf{k}'), \quad (4)$$

where $\Gamma_s(\mathbf{k}) = (1 + k/k_R)^{-1/2}$, and $k_R \sim R^{-1}$ plays the role of the interaction range in momentum space [29]. The Hamiltonian in Eq. (3) has three microscopic parameters: the effective mass m , the interaction strength V_s and range $R \sim k_R^{-1}$. As the density n is varied, we compare the interparticle spacing $\ell_{\text{ip}} = 1/\sqrt{n} = \sqrt{2\pi}/k_F$ to R and notice that the interactions are short-ranged when $R/\ell_{\text{ip}} \sim (k_F/k_R)(1/\sqrt{2\pi}) \ll 1$ and long-ranged when $R/\ell_{\text{ip}} \sim (k_F/k_R)(1/\sqrt{2\pi}) \gg 1$.

Effective Action: We consider the order parameter modulus $|\Delta|$ and its associated phase θ , to write the phase fluctuation effective action per band as [16]

$$S_{\text{eff}} = S_{\text{sp}}(|\Delta|) + S_{\text{ph}}(|\Delta|, \theta) + S_{\text{zp}}(|\Delta|, \theta) \quad (5)$$

The first term is the saddle-point action

$$S_{\text{sp}}(|\Delta|) = \sum_{\mathbf{k}} \left[\frac{(\xi_{\mathbf{k}} - E_{\mathbf{k}})}{T} - 2 \ln \left(1 + e^{-E_{\mathbf{k}}/T} \right) \right] + \frac{|\Delta|^2}{TV_s}, \quad (6)$$

where $E_{\mathbf{k}} = \sqrt{\xi_{\mathbf{k}}^2 + |\Delta_{\mathbf{k}}|^2}$ is the quasiparticle excitation energy, and $\Delta_{\mathbf{k}} = \Delta \Gamma_s(\mathbf{k})$ plays the role of the order parameter function for s -wave pairing. The second term is the phase fluctuation action

$$S_{\text{ph}} = \frac{1}{2} \int dr \left[\sum_{ij} \rho_{ij} \partial_i \theta(r) \partial_j \theta(r) + \kappa_s [\partial_\tau \theta(r)]^2 \right], \quad (7)$$

where the integration is over position and imaginary time $r = (\mathbf{r}, \tau)$, with $\int dr \equiv \int_0^{1/T} d\tau \int d^2\mathbf{r}$. In Eq. (7), the first term contains the superfluid density tensor

$$\rho_{ij}(\mu, |\Delta|, T) = \frac{1}{4L^2} \sum_{\mathbf{k}} [2n_{\text{sp}}(\mathbf{k}) \partial_i \partial_j \xi_{\mathbf{k}} - Y_{\mathbf{k}} \partial_i \xi_{\mathbf{k}} \partial_j \xi_{\mathbf{k}}], \quad (8)$$

where ∂_i denotes the partial derivative with respect to momentum k_i with $i = \{x, y\}$,

$$n_{\text{sp}}(\mathbf{k}) = \frac{1}{2} \left[1 - \frac{\xi_{\mathbf{k}}}{E_{\mathbf{k}}} \tanh \left(\frac{E_{\mathbf{k}}}{2T} \right) \right] \quad (9)$$

is the momentum distribution per spin state, and $Y_{\mathbf{k}} = (2T)^{-1} \text{sech}^2(E_{\mathbf{k}}/2T)$ is the Yoshida function. Here, the superfluid density tensor is diagonal since $\rho_{xy} = \rho_{yx} = 0$, and its diagonal elements are equal, that is, $\rho_{xx} = \rho_{yy} = \rho_s$. The second term in Eq. (7) is

$$\kappa_s(\mu, |\Delta|, T) = \frac{1}{4L^2} \sum_{\mathbf{k}} \left[\frac{|\Delta_{\mathbf{k}}|^2}{E_{\mathbf{k}}^3} \tanh \left(\frac{E_{\mathbf{k}}}{2T} \right) + \frac{\xi_{\mathbf{k}}^2}{E_{\mathbf{k}}^2} Y_{\mathbf{k}} \right], \quad (10)$$

with $\kappa_s = \kappa/4$, where $\kappa = \partial n / \partial \mu|_{T, V}$ is related to the thermodynamic compressibility $\mathcal{K} = \kappa/n^2$. The zero-point action is $S_{\text{zp}} = \sum_{\mathbf{q}} \omega_{\mathbf{q}}/2T$, where $\omega(\mathbf{q}) = c|\mathbf{q}|$ is the frequency and $c = \sqrt{\rho_s/\kappa_s}$ is the speed of sound.

To elucidate the role of phase fluctuations, we write $\theta(\mathbf{r}, \tau) = \theta_v(\mathbf{r}) + \theta_c(\mathbf{r}, \tau)$, where the classical (τ -independent) contribution $\theta_v(\mathbf{r})$ is due to vortices (transverse velocities), while the quantum (τ -dependent) contribution $\theta_c(\mathbf{r}, \tau)$ is due to collective modes (longitudinal velocities). The resulting phase action per band is

$$S_{\text{ph}} = S_v + S_c, \quad (11)$$

since contributions involving cross-terms in θ_v and θ_c vanish. The vortex action is

$$S_v = \frac{1}{2T} \int d^2\mathbf{r} \rho_s [\nabla \theta_v(\mathbf{r})]^2, \quad (12)$$

while the collective mode action is

$$S_c = \frac{1}{2} \int dr \left[\rho_s [\nabla \theta_c(r)]^2 + \kappa_s [\partial_\tau \theta_c(r)]^2 \right]. \quad (13)$$

The thermodynamic potential is $\Omega = \Omega_{\text{sp}} + \Omega_{\text{ph}}$, where the first term is the saddle-point $\Omega_{\text{sp}} = TS_{\text{sp}}$, and the second is due to phase fluctuations $\Omega_{\text{ph}} = \Omega_v + \Omega_c + \Omega_{\text{zp}}$.

The contribution due to vortices is $\Omega_v = -T \ln \mathcal{Z}_v$, where $\mathcal{Z}_v = \int d\theta_v e^{-S_v}$. Integration over phase fluctuations $\theta_c(\mathbf{r}, \tau)$ leads to $\Omega_c = \sum_{\mathbf{q}} T \ln [1 - \exp(-\omega_{\mathbf{q}}/T)]$, while the zero-point term is $\Omega_{zp} = TS_{zp}$.

Critical Temperature: The self-consistency relations for $|\Delta|$ and T_c for fixed chemical potential μ are derived from the effective action $S_{\text{eff}} = S_{\text{sp}} + S_{\text{ph}}$ as follows. The order parameter equation is obtained through the stationarity condition $\delta S_{\text{sp}}/\delta \Delta_0^* = 0$, leading to

$$\frac{1}{V_s} = \sum_{\mathbf{k}} \frac{|\Gamma_s(\mathbf{k})|^2}{2E_{\mathbf{k}}} \tanh\left(\frac{E_{\mathbf{k}}}{2T}\right). \quad (14)$$

The equation for the critical temperature $T_c = T_{\text{BKT}}$ is determined by the Kosterlitz-Thouless [3] condition

$$T_{\text{BKT}} = \frac{\pi}{2} \rho_s(\mu, |\Delta|, T_{\text{BKT}}), \quad (15)$$

obtained by using the vortex action of Eq. (12). For fixed interaction V_s and a given chemical potential μ , Eqs. (14) and (15) determine the order parameter modulus $|\Delta|$ and the critical temperature T_{BKT} . These two equations arise from the saddle-point and vortex actions.

To relate μ and $n = N/L^2$, where N is the total number of particles per band and L^2 is the area of the sample, we use $n = -\partial \bar{\Omega}/\partial \mu|_{T,V}$, with $\bar{\Omega} = \Omega/L^2$, leading to

$$n = n_{\text{sp}} + n_{\text{ph}} + n_{\text{zp}}. \quad (16)$$

Here, $n_j = -\partial \bar{\Omega}_j/\partial \mu|_{T,V}$ where $j = \{\text{sp}, \text{ph}, \text{zp}\}$. The expression of n_{sp} is particularly simple, that is, $n_{\text{sp}} = 2 \sum_{\mathbf{k}} n_{\text{sp}}(\mathbf{k})$, while the others can be easily obtained from their respective $\bar{\Omega}_j$. The self-consistent solutions of Eqs. (14), (15), and (16) determine μ , $|\Delta|$ and T_{BKT} as function of density n for given effective mass m , interaction strength V_s and momentum-space interaction range k_R . A measure of the evolution from BCS to Bose pairing is provided by the pair size [7]

$$\xi_{\text{pair}}^2 = \frac{\int d^2\mathbf{k} \varphi^*(\mathbf{k}) [-\nabla_{\mathbf{k}}^2] \varphi(\mathbf{k})}{\int d^2\mathbf{k} |\varphi(\mathbf{k})|^2} \quad (17)$$

in terms of the non-normalized two-body wavefunction $\varphi(\mathbf{k}) = \Delta(\mathbf{k})/2E(\mathbf{k})$.

We use momentum and energy scales k_R and $\varepsilon_R = k_R^2/2m$, respectively, and write the dimensionless order parameter equation as

$$\frac{1}{\tilde{V}_s} = \int d\tilde{k} \tilde{k} \frac{|\tilde{\Gamma}_s(\tilde{\mathbf{k}})|^2}{2\tilde{E}_{\tilde{\mathbf{k}}}} \tanh\left(\frac{\tilde{E}_{\tilde{\mathbf{k}}}}{2\tilde{T}}\right), \quad (18)$$

where $\tilde{V}_s = V_s g_{2D}$, with $g_{2D} = mL^2/\pi$ being the total 2D density of states per band. The dimensionless functions are $\tilde{\Gamma}_s(\tilde{\mathbf{k}}) = (1 + \tilde{k})^{-1/2}$ for the interaction symmetry factor, $\tilde{E}_{\tilde{\mathbf{k}}} = [\tilde{\xi}_{\tilde{\mathbf{k}}}^2 + |\tilde{\Delta}_{\tilde{\mathbf{k}}}|^2]^{1/2}$ for the quasiparticle excitation energy, with $\tilde{\xi}_{\tilde{\mathbf{k}}} = \tilde{k}^2 - \tilde{\mu}$ for the kinetic energy

and $\tilde{\Delta}_{\tilde{\mathbf{k}}} = \tilde{\Delta} \tilde{\Gamma}_s(\tilde{\mathbf{k}})$ for the order parameter function. The dimensionless critical temperature is

$$\tilde{T}_{\text{BKT}} = \frac{\tilde{n}_{\text{sp}}}{8} - \frac{1}{16\tilde{T}_{\text{BKT}}} \int d\tilde{k} \tilde{k}^3 \text{sech}^2\left(\frac{\tilde{E}_{\tilde{\mathbf{k}}}}{2\tilde{T}_{\text{BKT}}}\right), \quad (19)$$

where $\tilde{T}_{\text{BKT}} = T_{\text{BKT}}/T_R$, with $T_R = \varepsilon_R$. The dimensionless density $\tilde{n} = n/n_R$, where $n_R = k_R^2/2\pi$, is expressed solely in terms of the saddle-point contribution

$$\tilde{n} = \tilde{\varepsilon}_F = \tilde{n}_{\text{sp}} = \int d\tilde{k} \tilde{k} \left[1 - \frac{\tilde{\xi}_{\tilde{\mathbf{k}}}}{\tilde{E}_{\tilde{\mathbf{k}}}} \tanh\left(\frac{\tilde{E}_{\tilde{\mathbf{k}}}}{2\tilde{T}}\right) \right], \quad (20)$$

since n_{ph} and n_{zp} are small for $T \approx T_{\text{BKT}}$, except when n and/or $T \rightarrow 0$ [30]. For comparison, we also obtain the dimensionless mean field (MF) temperature $\tilde{T}_{\text{MF}} = T_{\text{MF}}/T_R$ by setting $|\tilde{\Delta}| = 0$ and solving only Eqs. (18) and (20), because MF neglects all phase fluctuations including the vortex-antivortex binding mechanism described by Eq. (19).

In Fig. 1, we show temperatures $\tilde{T}_{\text{BKT}} = T_{\text{BKT}}/T_R$, $\tilde{T}_{\text{MF}} = T_{\text{MF}}/T_R$, order parameter $|\tilde{\Delta}| = |\Delta|/\varepsilon_R$, chemical potential $\tilde{\mu} = \mu/\varepsilon_R$ and pair size $\xi_{\text{pair}} = k_R \xi_{\text{pair}}$ versus density $\tilde{n} = n/n_R$ for fixed $\tilde{V}_s = 0.7100$. Notice that $\tilde{n} = 2\pi(R/\ell_{\text{ip}})^2$ and a crossover from short- to long-ranged interactions occurs at $R/\ell_{\text{ip}} \sim 1$, that is, at $\tilde{n} \sim \tilde{n}_{\text{cr}} = 2\pi = 6.283$ as \tilde{n} grows. In Fig. 1(a), we show \tilde{T}_{BKT} and \tilde{T}_{MF} versus \tilde{n} and note that $\tilde{T}_{\text{MF}} \geq \tilde{T}_{\text{BKT}}$. The gray dotted line represents the upper bound $\tilde{T}_{\text{BKT}} = \tilde{n}/8 = \tilde{\varepsilon}_F/8$ discussed in the introduction [16]. Both \tilde{T}_{MF} and \tilde{T}_{BKT} are non-monotonic and have a maximum located at $\tilde{n} = 0.3241$ and $\tilde{n} = 0.5099$, respectively. The inclusion of phase fluctuations, via the BKT mechanism of vortex-antivortex binding, reduces T_{MF} to T_{BKT} through Eq. (19). Therefore the range $T_{\text{BKT}} < T < T_{\text{MF}}$ determines the region where classical phase fluctuations are important. In this region, preformed pairs are guaranteed to exist [31, 32]. However, we cannot interpret T_{MF} as the experimental pseudogap temperature T^* defined as a 1% drop in the zero-bias conductance [28]. The theoretical understanding of T^* requires further analysis [33].

In Fig. 1(b), we show the $|\tilde{\Delta}|$ versus \tilde{n} both at $\tilde{T} = \tilde{T}_{\text{BKT}}$ and $\tilde{T} = 0$, noticing that $|\tilde{\Delta}|$ at $\tilde{T} = \tilde{T}_{\text{BKT}}$ has a maximum at $\tilde{n} = 0.1939$, while $|\tilde{\Delta}|$ at $\tilde{T} = 0$ has a maximum at $\tilde{n} = 0.4356$. In Fig. 1(c), we show $\tilde{\mu}$ versus \tilde{n} both at $\tilde{T} = \tilde{T}_{\text{BKT}}$ and $\tilde{T} = 0$, observing that $\tilde{\mu}$ is a monotonically increasing function of \tilde{n} as expected. For higher densities, where the superconductor is deep in the degenerate BCS regime, $\tilde{\mu} \rightarrow \tilde{\varepsilon}_F = \tilde{n}$, as indicated by the gray dot-dashed line. For lower densities, where the superconductor is deep in the non-degenerate Bose regime, $\tilde{\mu} \rightarrow -|\tilde{E}_B|/2 = -0.004309$ as indicated by the gray dotted line. Here, $\tilde{E}_B = -0.008619$ is the dimensionless binding energy obtained from the two-body

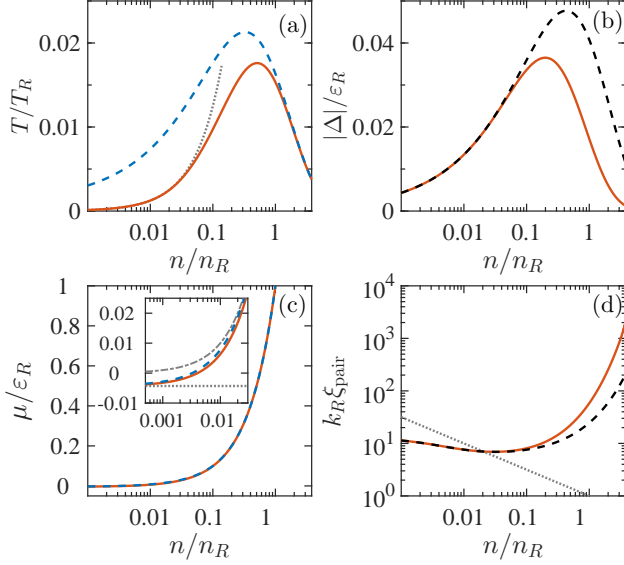


FIG. 1. The coupling constant is $\tilde{V}_s = 0.7100$ in all panels. (a) Temperatures \tilde{T}_{BKT} (red solid line), \tilde{T}_{MF} (blue dashed line) and upper bound $\tilde{T}_{\text{BKT}} = \tilde{\varepsilon}_F/8 = \tilde{n}/8$ (gray dotted line) vs \tilde{n} . (b) Order parameter $|\Delta|$ vs \tilde{n} at $\tilde{T} = \tilde{T}_{\text{BKT}}$ (red solid line) and $\tilde{T} = 0$ (black dashed line). (c) Chemical potential $\tilde{\mu}$ vs \tilde{n} at $\tilde{T} = \tilde{T}_{\text{BKT}}$ (red solid line) and $\tilde{T} = T_{\text{MF}}$ (blue dashed line). Inset: $\tilde{\mu} = \tilde{\varepsilon}_F = \tilde{n}$ (gray dot-dashed line) and $\tilde{\mu} = -|\tilde{E}_B|/2$ (gray dotted line). (d) Pair size $\tilde{\xi}_{\text{pair}}$ vs \tilde{n} at $\tilde{T} = \tilde{T}_{\text{BKT}}$ (red solid line), $\tilde{T} = 0$ (black dashed line), and $\tilde{\xi}_{\text{pair}} = \tilde{n}^{-1/2}$ (gray dotted line), that is, $k_F \xi_{\text{pair}} = 1$ at $\tilde{T} = 0$.

bound state eigenvalue equation [16]

$$\frac{1}{\tilde{V}_s} = \int d\tilde{k} \tilde{k} \frac{|\tilde{\Gamma}_s(\tilde{\mathbf{k}})|^2}{2\tilde{k}^2 - \tilde{E}_B}. \quad (21)$$

for $\tilde{V}_s = 0.7100$. Spectroscopically, the BCS-Bose crossover occurs at $\tilde{\mu} = 0$ ($\tilde{n} = 0.004032$), where the gap for quasiparticle excitations changes from $\tilde{E}_g = |\tilde{\Delta}|$ on the BCS-pairing side ($\tilde{n} > 0.004032$) to $\tilde{E}_g = \sqrt{\tilde{\mu}^2 + |\tilde{\Delta}|^2}$ on the Bose-pairing side ($\tilde{n} < 0.004032$).

In Fig. 1(d), we show that the pair size $\tilde{\xi}_{\text{pair}} = k_R \xi_{\text{pair}}$ is not a monotonically increasing function of \tilde{n} , having a minimum at $\tilde{n} = 0.03275$. We emphasize that ξ_{pair} is not the phase coherence length ξ_{ph} that diverges at the BKT transition, but it provides a measure that the BCS-Bose pairing crossover region occurs when $k_F \xi_{\text{pair}} \sim 1$ [31]. The condition $k_F \xi_{\text{pair}} = 1$ or $\tilde{\xi}_{\text{pair}} = \tilde{k}_F^{-1} = \tilde{n}^{-1/2}$ is represented by the gray dotted line. The BCS-pairing limit corresponds to $\tilde{\xi}_{\text{pair}} \gg \tilde{n}^{-1/2}$, that is, $k_F \xi_{\text{pair}} \gg 1$. In contrast, the Bose-pairing limit corresponds to $\tilde{\xi}_{\text{pair}} \ll \tilde{n}^{-1/2}$, that is, $k_F \xi_{\text{pair}} \ll 1$.

In Fig. 2, we compare our theoretical results for T_{BKT} , $|\Delta|$, μ , and ξ_{pair} to experimental results for Li_xZrNCl [28]. In Figs. 2(a) and (b), we vary the dimensionless coupling constant \tilde{V}_s to match the theoreti-

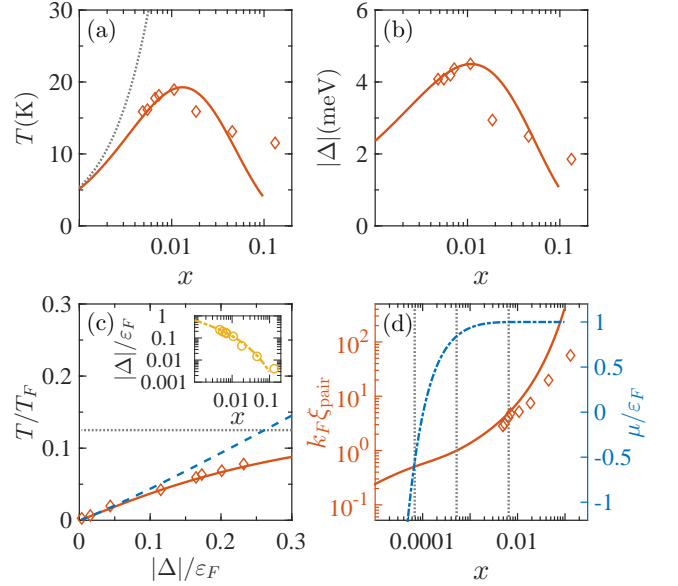


FIG. 2. Theoretical parameters are $\tilde{V}_s = 0.7100$, $T_R = 1094\text{K}$, $k_R = 0.4310/a$. Experimental data [28] (red diamonds and yellow circles). (a) T (in K) vs x , theoretical T_{BKT} (red solid line). (b) $|\Delta|$ (in meV) at $T = 2\text{K}$, theoretical $|\Delta|$ (red solid line). (c) T/T_F vs $|\Delta|/\varepsilon_F$, T_{BKT}/T_F (red solid line), T_{MF}/T_F (blue dashed line), and $T_{\text{BKT}}/T_F = 1/8 = 0.125$ (gray dotted line). Inset: $|\Delta|$ vs x , theoretical (yellow dot-dashed line). (d) Theoretical $k_F \xi_{\text{pair}}$ (red solid line), experimental $k_F \xi_{\text{exp}}$ (red diamonds) both at $T = 0$; μ/ε_F (blue dot-dashed line) at $T = T_{\text{BKT}}$. The vertical gray dotted lines at $x = \{6.549 \times 10^{-5}, 5.238 \times 10^{-4}, 6.564 \times 10^{-3}\}$ give $k_F \xi_{\text{pair}} = \{0.5, 1.0, 5.0\}$.

cal T_{BKT} and $|\Delta|$ to the experimental T_c and $|\Delta|$ versus concentration x . The best fit is achieved for $\tilde{V}_s = 0.7100$, and from it we extract the temperature scale $T_R = \varepsilon_R = k_R^2/2m$ leading to $T_R = 1094\text{K}$ and the momentum scale k_R by relating \tilde{n} to x , that is, by using the carrier density per band $n = x/A_{\text{cell}}$, where $A_{\text{cell}} = a^2 \sin(\pi/3)$ is the area of the unit cell of Li_xZrNCl . In this case, $\tilde{n} = 2\pi x/k_R^2 A_{\text{cell}}$, and the momentum scale from the fit is $k_R = 0.4310/a = 1.197\text{nm}^{-1}$, where $a = 0.3601\text{nm}$ is the characteristic length of the unit cell. Note that the interaction range $R \sim 1/k_R = 2.320a = 0.8354\text{nm}$ spans a few lattice spacings, suggesting that the extension to a lattice model should require interactions involving only a few neighbors. The effective mass m is obtained from $m = k_R^2/2\varepsilon_R$ leading to $m = 0.5791m_e$, where m_e is the bare electron mass, in good agreement with band structure calculations [34, 35]. Since $\tilde{n} = 2\pi(R/\ell_{\text{ip}})^2$, the crossover from short- to long-ranged interactions occurs at $R/\ell_{\text{ip}} \sim 1$, that is, $\tilde{n} \sim \tilde{n}_{\text{cr}} = 2\pi$ ($x \sim 0.1608$), meaning that interactions are sufficiently short-ranged over the experimental range, however a non-zero R is absolutely essential in producing a maximum in T_{BKT} versus x .

In Fig. 2(b), we show $|\Delta|$ (in meV) at $T = 2\text{K}$ versus x . The red diamonds are the experimental data, and the red solid line are theoretical results using the

same values of T_R , k_R and \tilde{V}_s given in Fig. 2(a). In Fig. 2(c), we show T_{BKT}/T_F and T_{MF}/T_F versus $|\Delta|/\varepsilon_F$ at $T = 2\text{K}$ for the same values of T_R , k_R and \tilde{V}_s . The upper bound $T_{\text{BKT}} = 0.125T_F$ [16] is the gray dotted line. The range $T_{\text{BKT}}/T_F < T/T_F < T_{\text{MF}}/T_F$ determines the region where phase fluctuations are important. The inset shows $|\Delta|/\varepsilon_F$ versus x comparing experiment (yellow circles) and theory (yellow dot-dashed line). In Fig. 2(d), we show $k_F\xi_{\text{pair}}$ and μ/ε_F versus x . The theoretical $k_F\xi_{\text{pair}}$ is compared with the experimental $k_F\xi_{\text{exp}}$ [36] at $T = 0$, while the theoretical μ/ε_F is at $T = T_{\text{BKT}}$. The vertical gray dotted lines at $x = \{6.549 \times 10^{-5}, 5.238 \times 10^{-4}, 6.564 \times 10^{-3}\}$ give $k_F\xi_{\text{pair}} = \{0.5, 1.0, 5.0\}$. The crossover region from BCS to Bose pairing occurs in the range $0.5 < k_F\xi_{\text{pair}} < 5.0$ or $6.549 \times 10^{-5} < x < 6.564 \times 10^{-3}$, with corresponding $-0.6113 < \mu/\varepsilon_F < 0.9995$. At the lowest experimental concentration $x = 0.0048$, we find $k_F\xi_{\text{pair}} = 3.826$ and $\mu/\varepsilon_F = 0.9979$, showing that the crossover region has just been entered. Our results demonstrate that the Bose pairing regime has not yet been reached experimentally for gated 2D Li_xZrNCl , as it requires $x < 6.549 \times 10^{-5}$, $k_F\xi_{\text{pair}} < 0.5$ and $\mu/\varepsilon_F < -0.6113$.

Final Remarks: Our theoretical work shows good agreement with experimental data in the range $0.0048 \leq x \leq 0.133$ [28]. However, for $x \geq 0.1$ there are some deviations which our current model does not capture as described next. First, according to Ref. [28], for $x \geq 0.1$ there is a crossover in behavior from two to three dimensions, which our strictly 2D model does not include. Second, it was suggested [28] that electron-phonon interactions may play a role specially for $x \geq 0.1$, but our model does not include retardation effects. Third, for $x \geq 0.1$, our results suggest that it is necessary to include band-structure effects (non-parabolicity of bands) with a corresponding increase in the density of states that leads to an increase in T_c , $|\Delta|$ and a decrease in $k_F\xi_{\text{pair}}$.

Conclusions: We investigated a density induced evolution from BCS to Bose pairing in gated two-dimensional superconductors with two degenerate parabolic bands and showed that there is good agreement with experimental results [28] of Li_xZrNCl for $x \leq 0.1$, where the effective mass approximation is valid. We conclude that, at the lowest reported concentration $x = 0.0048$, the chemical potential is still very close to the Fermi energy, and that the pair size is $k_F\xi_{\text{pair}} = 3.826$, indicating that experiments have just entered the crossover region from the BCS-side. We suggest that it is necessary to reduce the lowest concentration by at least one order of magnitude to start entering the Bose pairing regime experimentally.

We thank Yoshiro Iwasa for discussions, and the National Key R&D Program of China (Grant 2018YFA0306501), the National Natural Science Foundation of China (Grants 11522436 & 11774425), the Beijing Natural Science Foundation (Grant Z180013), and the Research Funds of Renmin University of China (Grants

16XNLQ03 & 18XNLQ15) for financial support.

* wzhangl@ruc.edu.cn

† carlos.sademelo@physics.gatech.edu

- [1] A. M. Goldman, The Berezinskii-Kosterlitz-Thouless transition in superconductors, In 40 years of the Berezinskii-Kosterlitz-Thouless theory, 135, World Scientific (2013).
- [2] V. L. Berezinskii, Destruction of long-range order in one-dimensional and two-dimensional systems having a continuous symmetry group : I. Classical systems. Sov. Phys. JETP **32**, 493 (1970).
- [3] J. M. Kosterlitz and D. Thouless, Long-range order and metastability in two dimensional solids and superfluids: Application of dislocation theory. J. Phys. C **5**, L124 (1972)
- [4] M. R. Beasley, J. E. Mooij, and T. P. Orlando, Phys Possibility of Vortex-antivortex pair dissociation in two-dimensional superconductors, Rev. Lett. **42**, 1165 (1979).
- [5] K. Epstein, A. M. Goldman, and A. M. Kadin, Vortex-antivortex pair dissociation in two-dimensional superconductors, Phys. Rev. Lett. **47**, 534 (1981).
- [6] B. I. Halperin and D. R. Nelson, Resistive transition in superconducting films, J. Low Temp. Phys. **36**, 599 (1979).
- [7] R. D. Duncan and C. A. R. Sá de Melo, Thermodynamic properties in the evolution from BCS to Bose-Einstein condensation for a d-wave superconductor at low temperatures, Phys. Rev. B **62**, 9675 (2000).
- [8] S. S. Botelho and C. A. R. Sá de Melo, Lifshitz transition in d-wave superconductors, Phys. Rev B **71**, 134507 (2005).
- [9] N. Read and D. Green, Paired states of fermions in two dimensions with breaking of parity and time-reversal symmetries and the fractional quantum Hall effect, Phys. Rev. B **61**, 10267 (2000)
- [10] S. S. Botelho and C. A. R. Sá de Melo, Quantum Phase Transition in the BCS-to-BEC Evolution of p-wave Fermi Gases, J. Low Temp. Phys. **140**, 409 (2005).
- [11] C. H. Ahn, J.-M. Triscone, and J. Mannhart, Electric field effect in correlated oxide systems, Nature **424**, 1015, (2003).
- [12] D. Matthey, S. Gariglio, C.H. Ahn, and J.-M. Triscone, Electrostatic modulation of the superconducting transition in thin $\text{NdBa}_2\text{Cu}_3\text{O}_{7-\delta}$ films: The role of classical fluctuations. Physica C **583**, 372, (2002).
- [13] V. J. Emery and S. A. Kivelson, Importance of phase fluctuations in superconductors with small superfluid density, Nature **374**, 434 (1995).
- [14] Y. J. Uemura, G. M. Luke, B. J. Sternlieb, J. H. Brewer, J. F. Carolan, W. N. Hardy, R. Kadono, J. R. Kempton, R. F. Kiefl, S. R. Kreitzman, P. Mulhern, T. M. Rise-man, D. Li. Williams, B. X. Yang, S. Uchida, H. Takagi, J. Gopalakrishnan, A. W. Sleight, M. A. Subramanian, C. L. Chien, M. Z. Cieplak, Gang Xiao, V. Y. Lee, B. W. Statt, C. E. Stronach, W. J. Kossler, and X. H. Yu, Universal Correlations between T_c and n_s/m^* (carrier density over effective mass) in high- T_c cuprate superconductors, Phys. Rev. Lett. **62**, 2317 (1989).
- [15] Y. J. Uemura, L. P. Le, G. M. Luke, B. J. Sternlieb, W.

- D. Wu, J. H. Brewer, T. M. Riseman, C. L. Seaman, M. B. Maple, M. Ishikawa, D. G. Hinks, J. D. Jorgensen, G. Saito, and H. Yamochi, Basic similarities among cuprate, bismuthate, organic, Chevrel-phase, and heavy-fermion superconductors shown by penetration-depth measurements, *Phys. Rev. Lett.* **66**, 2665 (1991).
- [16] S. S. Botelho and C. A. R. Sá de Melo, Vortex-Antivortex Lattice in Ultracold Fermionic Gases, *Phys. Rev. Lett.* **96**, 040404 (2006).
- [17] R. A. Ferrell and R. E. Glover, Conductivity of superconducting films: A sum rule, *Phys. Rev.* **109**, 1398 (1958).
- [18] M. Tinkham and R. A. Ferrell, Determination of the superconducting skin depth from the energy gap and sum rule, *Phys. Rev. Lett.* **2**, 331 (1959).
- [19] M. Tinkham, *Introduction to Superconductivity*, McGraw-Hill, New York, 1975.
- [20] J. P. A. Devreese, J. Tempere and Carlos A. R. Sá de Melo, Effects of Spin-Orbit Coupling on the Berezinskii-Kosterlitz-Thouless Transition and the Vortex-Antivortex Structure in Two-Dimensional Fermi Gases, *Phys. Rev. Lett.* **113**, 165304 (2014).
- [21] J. P. A. Devreese, J. Tempere, and C. A. R. Sá de Melo, Quantum phase transitions and Berezinskii-Kosterlitz-Thouless temperature in a two-dimensional spin-orbit-coupled Fermi gas, *Phys. Rev. A* **92**, 043618 (2015).
- [22] S. Kasahara, T. Watashige, T. Hanaguri, Y. Kohsaka, T. Yamashita, Y. Shimoyama, Y. Mizukami, R. Endo, H. Ikeda, K. Aoyama, T. Terashima, S. Uji, T. Wolf, H. von Löhneysen, T. Shibauchi, and Y. Matsuda, Field-induced superconducting phase of FeSe in the BCS-BEC crossover, *Proc. Natl. Acad. Sci. U.S.A.* **111**, 16309–16313 (2014).
- [23] S. Rinott, K. B. Chashka, A. Ribak, E. D. L. Rienks, A. Taleb-Ibrahimi, P. Le Fevre, F. Bertran, M. Randeria and A. Kanigel, Tuning across the BCS-BEC crossover in the multiband superconductor $\text{Fe}_{1+y}\text{Se}_x\text{Te}_{1-x}$: An angle-resolved photoemission study, *Sci. Adv.* **3**, e1602372 (2017).
- [24] T. Hashimoto, Y. Ota, A. Tsuzuki, T. Nagashima, A. Fukushima, S. Kasahara, Y. Matsuda, K. Matsuura, Y. Mizukami, T. Shibauchi, S. Shin, and K. Okazaki, Bose-Einstein condensation superconductivity induced by disappearance of the nematic state, *Sci. Adv.* **6**, eabb9052 (2020).
- [25] Y. Cao, V. Fatemi, S. Fang, K. Watanabe, T. Taniguchi, E. Kaxiras, and P. Jarillo-Herrero, Unconventional superconductivity in magic-angle graphene superlattices, *Nature* **556**, 43 (2018).
- [26] J. M. Park, Y. Cao, K. Watanabe, T. Taniguchi, P. Jarillo-Herrero, Tunable strongly coupled superconductivity in magic-angle twisted trilayer graphene, *Nature* **590**, 249–255 (2021).
- [27] Y. Nakagawa, Y. Saito, T. Nojima, K. Inumaru, S. Yamanaka, Y. Kasahara, and Y. Iwasa, Gate-controlled low carrier density superconductors: Toward the two-dimensional BCS-BEC crossover *Phys. Rev. B* **98**, 064512 (2018).
- [28] Yuji Nakagawa, Yuichi Kasahara, Takuya Nomoto, Ryotaro Arita, Tsutomu Nojima, Yoshihiro Iwasa, Gate-controlled BCS-BEC crossover in a two-dimensional superconductor, *Science* **372**, 190–195 (2021).
- [29] This parametrization is necessary to produce a separable potential in momentum space that behaves both at small and large momenta in a form that is compatible to an acceptable real space interaction potential $V(\mathbf{r}, \mathbf{r}')$, as previously investigated in the literature [7].
- [30] Additional contributions to the number equation beyond phase fluctuations also arise in the Bose limit (low densities) and lead to logarithmic corrections of T_{BKT} due to residual boson-boson interactions. See, e.g., D. S. Fisher, and P. C. Hohenberg, Dilute Bose gas in two dimensions, *Phys. Rev. B* **37**, 4936 (1988).
- [31] C. A. R. Sá de Melo, M. Randeria, and J. R. Engelbrecht, Crossover from BCS to Bose superconductivity: Transition temperature and time-dependent Ginzburg-Landau theory, *Phys. Rev. Lett.* **71**, 3202 (1993).
- [32] C. A. R. Sá de Melo, When fermions become bosons: Pairing in ultracold gases, *Physics Today*, October issue, 45 (2008).
- [33] For $T > T_{\text{MF}}$, where $|\Delta| = 0$, fermions still interact and cannot be treated as free particles. Since there is always a two-body bound state in two dimensions for an arbitrary small attractive interaction, these bound states must be included for $T > T_{\text{MF}}$ and the density of fermions needs to be separated at least into bound (preformed pairs) and unbound contributions. To recover bound fermions above T_{MF} it is necessary to include amplitude fluctuations of Δ . Therefore, T^* is related to the Saha dissociation temperature T_S , where a fraction of preformed pairs B dissociates into two fermions F_\uparrow and F_\downarrow with opposite spins, satisfying the chemical equilibrium equation $B \rightleftharpoons F_\uparrow + F_\downarrow$. Details of this analysis will be investigated in a future publication.
- [34] R. Weht, A. Filippetti, W. E. Pickett, Electron doping in the honeycomb bilayer superconductors $(\text{Zr}, \text{Hf})\text{NCl}$, *Europhys. Lett.* **48**, 320–325 (1999).
- [35] R. Heid, K. P. Bohnen, Ab Initio lattice dynamics and electron-phonon coupling in Li_xZrNCl . *Phys. Rev. B* **72**, 134527 (2005).
- [36] The experimental parameter ξ_{exp} is extracted from the measurement of the temperature dependent of the upper critical field $H_{c2}(T)$ using the Ginzburg-Landau relation $H_{c2}(T) = \Phi_0/2\pi\xi^2(T)$, with $\xi(T) = \xi_{\text{exp}}(1 - T/T_c)^{-1/2}$ and extrapolating it to $T = 0$, from $H_{c2}(T) = (\Phi_0/2\pi\xi_{\text{exp}}^2)(1 - T/T_c)$ for $T < T_c$. Here Φ_0 is the flux quantum $\hbar c/2e$, and T_c is the zero-field critical temperature. The experimental value $\xi_{\text{exp}} = [2\pi H_{c2}(0)/\Phi_0]^{1/2}$ and the theoretical values of ξ_{pair} are in good agreement in the range $0 \leq x \leq 0.1$, where the system is expected to be in the truly 2D regime [28], band structure (lattice) effects are not important, and the experimental system is closer to the BCS-pairing side of the crossover. At the Bose-pairing side of the crossover is approached, we expect substantial deviations between ξ_{pair} and ξ_{exp} as discussed in the three-dimensional version of the BCS-BEC crossover [31].